ECEE2026
18th European Conference on Earthquake Engineering

Optimisation of a Buckling-Delayed Shear Link Dissipation System

J. Ramirez [1,2], J. Gonzalez[1,2], L. Lazaro[1], F. Rastellini[1,2], G. Bozzo[2,3], L. Bozzo[4], J. Irazabal[1]

1- Centre Internacional en Metodes Numèrics en Enginyeria (CIMNE). Barcelona, Spain
2- Universitat Politècnica de Catalunya (UPC). Barcelona, Spain.
3- SLB Devices. Barcelona, Spain. info@slbdevices.com
4- Luis Bozzo Estructuras y Proyectos S. L. Barcelona, Spain.

{jramirez, llazaro, frastellini, jirazabal}@cimne.upc.edu,
jose.manuel.gonzalez@upc.edu,
info@slbdevices.com
lbozrot@ciccp.es

Abstract

This study proposes a geometric optimisation strategy for a buckling-delayed shear link (BDSL) dissipator based on a combined assessment of global response and local damage-related indicators. A three-dimensional numerical model, previously calibrated against experimental cyclic tests, is employed to evaluate the hysteretic behaviour, energy dissipation capacity, and local strain evolution of the device. The proposed approach combines a triaxiality-based failure indicator, namely the Triaxial Failure Map (TFM) index, with the evolution of local strain fields to identify critical regions susceptible to damage and to interpret the associated failure mechanisms. In particular, shear strains in the dissipative windows and longitudinal strains in the surrounding frame are analysed to control the distribution of inelastic demand and to reduce the risk of premature instability. The optimisation process focuses on modifying the window geometry and the main dimensions of the dissipator to improve the balance of the TFM index among the structural components. The results show that the optimised configurations promote a more uniform distribution of plastic strains across the dissipative windows, enhance the efficiency of the energy dissipation mechanism, and reduce damage concentration in the frame, leading to a more stable cyclic response. Overall, the proposed methodology provides a consistent design framework for dissipative devices with improved damage control and energy dissipation performance under seismic loading..

Keywords: Buckling-delayed Shear Link, Seismic energy dissipation, Triaxial Failure Map, Nonlinear plastic behaviour, Geometric and stiffness optimization

1- INTRODUCTION

Shear link dissipators are commonly employed in seismic energy dissipation systems due to their stable hysteretic response and capacity to localise inelastic deformations in replaceable components [1, 2]. These devices improve the ductility of structures and lower the seismic demand on primary members by encouraging controlled yielding under cyclic loading. Among these systems, modified shear link configurations have been proposed to improve cyclic stability and delay local buckling through geometric optimisation and stiffness redistribution [2].

Despite their favourable global performance, the behaviour of shear link systems is governed by local stress and strain conditions that can initiate damage. Under cyclic loading, the interaction between stress triaxiality η and accumulated plastic deformation governs the progression of damage, leading to localisation, instability, and premature low-cycle fatigue failure. [3, 4]. In addition, the local response arises from the interaction between shear-dominated plasticity in the dissipative regions and flexural effects in the surrounding frame, leading to deformation patterns that cannot be captured through global indicators alone. Consequently, conventional design approaches based on global quantities, including force–displacement response, peak strength, and cumulative dissipated energy, may not fully capture the mechanisms that control behaviour and potential failure.

Advanced nonlinear finite element modelling enables a detailed assessment of stress states and strain evolution in dissipative devices. Stress triaxiality is widely recognised as a key parameter influencing damage initiation and failure mechanisms in structural steel under cyclic loading [4–6]. Failure loci defined in terms of equivalent plastic strain and stress triaxiality provide a consistent framework for characterising stress-state-dependent behaviour [5–7] and linking plastic deformation to hydrostatic stress conditions. Rather than serving as explicit fracture models, these approaches can be used as indicators to assess the susceptibility of different regions to damage. At the same time, an accurate description of the structural response requires evaluating

local strain components, including shear and longitudinal plastic strains, to capture the interaction among deformation mechanisms.

Previous work developed and validated a three-dimensional nonlinear finite element model of the BDSL device under cyclic loading [8,9]. In parallel, Rastellini et al. [10] introduced a Triaxial Failure Diagram for multiaxial stress states in sheet-metal forming; in the present work, that concept is adapted as a post-processing indicator for BDSL assessment. However, the use of this framework for structural design remains limited. In particular, the combined evaluation of triaxiality-based indicators and local plastic strain demands within a systematic parametric investigation has received limited attention. The interaction between shear-dominated plasticity, longitudinal strain components, and geometric parameters—such as window thickness, number of windows, and global proportions—requires further investigation to establish robust design criteria.

Building on this validated framework, the present study investigates BDSL behaviour from a combined energy- and damage-based perspective. A parametric investigation is conducted to examine variations in key geometric and stiffness parameters. The Triaxial Failure Map (TFM) index is used together with shear and longitudinal plastic strain demands to identify critical stress states and local deformation concentrations [10]. Based on this information, a geometric optimisation strategy is proposed to improve the distribution of inelastic demand, enhance cyclic behaviour, and keep damage screening indicators within the adopted design thresholds. This approach provides a consistent mechanical basis for the structural design of buckling-delayed shear link dissipators under cyclic loading.

The novelty of the present study does not lie in the development of a new constitutive or fracture model, but in the design-oriented use of a previously validated BDSL numerical model. Specifically, the contribution of this paper is the systematic combination of TFM-based indicators and local strain metrics to guide the redistribution of window thickness and to assess the balance between energy dissipation and damage concentration.

2- BUCKLING-DELAYED SHEAR LINK

The Buckling-Delayed Shear Link (BDSL) system consists of a steel dissipative element integrated within a rigid frame. It is connected through a mechanism that prevents axial force transmission while allowing in-plane rotation [11], as illustrated in Figure 1. Figure 1a shows its application as a shear energy dissipation device in structural systems, integrated above reinforced concrete panels. Figure 1b illustrates the specimen detail. Figure 1c provides a schematic representation of the main components and geometric parameters. At the top of the system, a connector aligns the actuator with a mechanical slot. This allows displacement to be applied while preventing axial force transmission. As a result, the response is primarily governed by shear.

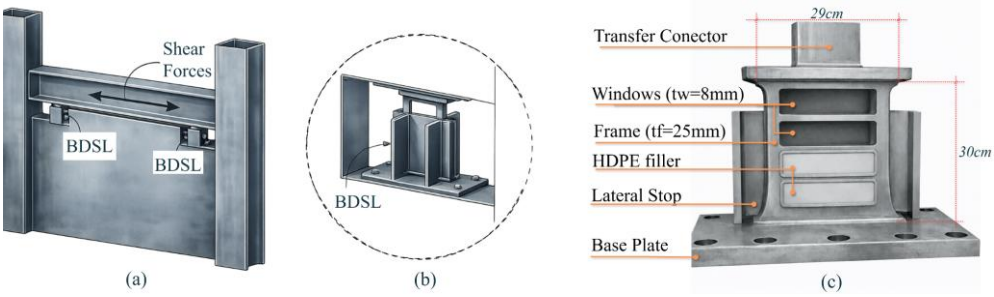

Figure 1 – Buckling-Delayed Shear Link (BDSL): (a) structural implementation; (b) detailed view of the specimen; (c) schematic representation of geometry and components.

Energy dissipation is governed by controlled yielding in reduced-thickness regions, referred to as windows, which are symmetrically distributed along the web of the device. These regions concentrate plastic deformations, while the overall configuration of the device delays the onset of local and global buckling. The dissipative element consists of a central steel component in which inelastic deformations develop under cyclic loading. In the middle region of the link, four rectangular windows are vertically aligned, reducing stiffness and guiding the deformation pattern. The windows have a uniform thickness of 8 mm, while the surrounding frame has a constant thickness of 25 mm, resulting in a symmetric configuration.

The windows can be filled with high-density polyethylene (HDPE) inserts. These inserts act as a deformable filler. They provide lateral support and help control local buckling. The specimen is anchored to a rigid base plate through bolted connections. In addition, lateral confinement blocks are placed on both sides of the link. These blocks restrict out-of-plane displacements and prevent lateral instability.

This configuration enables the investigation of cyclical behaviours under severe loading conditions. The influence of key geometric parameters is evaluated, including the stiffness reduction introduced by the number

of windows, their thickness, and the main dimensions of the dissipator. For the present study, a simplified nomenclature of the form *H_B_tf* (dimensions in cm) is adopted, where *H* represents the window height, *B* is the width of the dissipator, and *tf* is the thickness of the surrounding frame. This notation ensures consistency when performing geometric modifications at the volumetric level.

3- NUMERICAL FRAMEWORK, MODEL VALIDATION AND MECHANICAL ANALYSIS

This study employs a three-dimensional numerical model previously developed and validated against experimental cyclic tests [9, 12]. The model is implemented in the Compack solver, a computational tool for dynamic analysis based on an explicit time integration scheme (Fig. 2a) [13]. A total Lagrangian formulation with geometric and material nonlinearities is adopted [14]. The cyclic behaviour of ASTM A36 steel is reproduced using a calibrated Yoshida–Uemori model [15, 16]. The discretisation uses a structured mesh of linear 8-node hexahedral elements with reduced Gauss integration, which accurately captures the shear and volumetric responses.

The mesh discretisation, the main components, and the buckling control system are presented in Figures 2b and 2c. All contact interactions in the simulation are modelled using a penalty-based algorithm [17]. In particular, the contact between the actuator and the upper connector reproduces the axial release mechanism, allowing displacement transfer while preventing axial force transmission. As a result, the response is governed by shear-dominated deformations, with plastic strains localised within the dissipative windows.

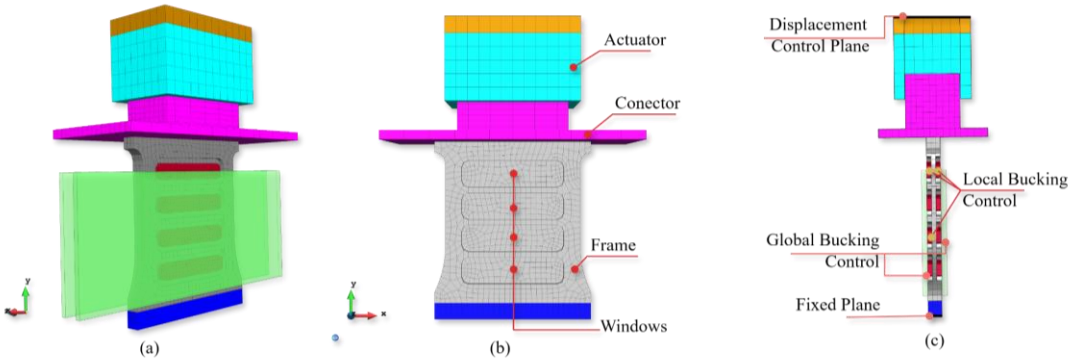

Figure 2 – Finite element model of the BDSL device: (a) mesh discretisation, (b) main components, and (c) boundary conditions with local and global buckling control.

After calibrating the constitutive parameters, the numerical model shows excellent agreement with the experimental response. It captures the hysteretic behaviour (Fig. 3a), cumulative energy dissipation (Fig. 3b), and the skeleton curve, including the failure point (Fig. 3c). The modelling strategy and validation are described in detail elsewhere [8, 9], and the validated framework is adopted here as a reliable basis for the subsequent analyses.

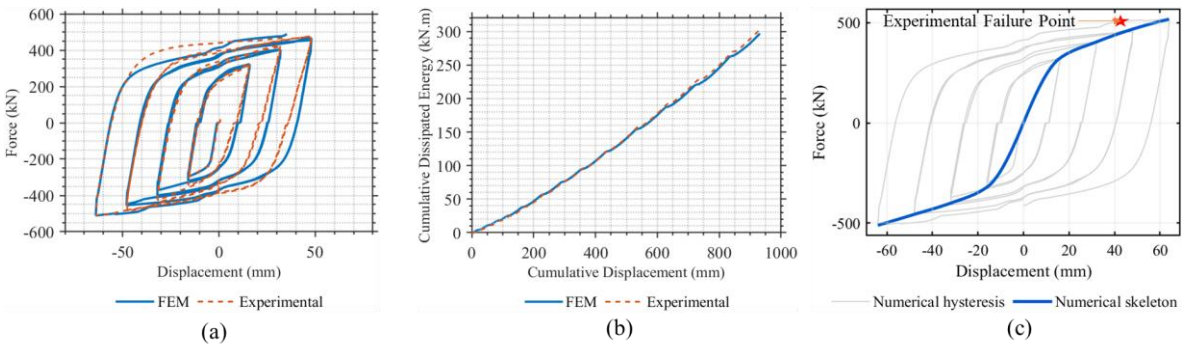

Figure 3 – Numerical validation: (a) hysteretic response, (b) cumulative energy, and (c) skeleton curve.

To evaluate failure-related behaviours, a Triaxial Failure Map (TFM) is used. The TFM is defined based on a Triaxial Failure Curve (TFC), which describes the relationship between Equivalent Plastic Strain and stress triaxiality η at failure [18]. This framework allows assessing the evolution of the stress state within the dissipative element and identifying conditions approaching ductile fracture. The resulting indicator, referred to as the triaxial failure index (TFM index), quantifies the proximity of the material state to the failure envelope and is not part of the constitutive model. For each integration point, stress triaxiality η and equivalent plastic

strain are computed throughout the loading history and compared with the TFC to evaluate the evolution of the material state.

The optimisation problem is defined as the maximisation of dissipated energy, subject to: (i) $TFM\_frame \leq 100$, (ii) target $80 \leq TFM\_window \leq 90$, (iii) bounded longitudinal strain in the frame, and (iv) practical geometric limits on window thickness. The design variables are the window thicknesses $tw(i)$, the number of windows, and the baseline geometry B. Candidate solutions are explored through a discrete parametric search over N configurations.

The spatial distribution of the TFM index within the specimen is shown in Figure 4a, and it is consistent with the experimentally observed failure regions. A threshold value of 120 is adopted here as a comparative screening limit, calibrated against the observed failure-prone regions of the reference configuration; it should not be interpreted as a universal failure threshold. High concentrations are observed in specific windows, particularly in the third window from top to bottom, as well as in the frame at approximately one third of its height, near the section transition in the curved region. The corresponding strain–triaxiality states at all integration points, together with the TFC, are shown in Figure 4b. The results show that points located in the windows are governed by shear-dominated conditions, with stress triaxiality η close to $-1/3$, while points in the frame are subjected to higher triaxiality levels and more demanding stress states. This representation allows tracking the evolution of the material state relative to the ductile fracture limit

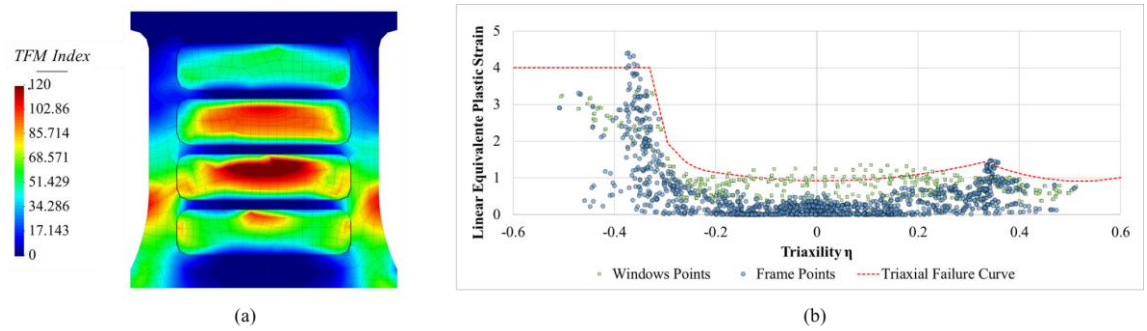

Figure 4 – TFM index: (a) spatial distribution, (b) strain–triaxiality η states relative to the TFC curve.

In addition to the TFM index, local deformation demand is characterised using supplementary strain indicators. The shear plastic strain εxy is monitored in the window regions, while the longitudinal strain εyy is analysed to capture bending effects in the frame. Figure 5a shows the concentration of deformation in the windows, and Figure 5b presents the evolution of strains in both the windows and the surrounding frame. Peak shear strain εxy reaches approximately 0.10, while longitudinal strain εyy attains values close to 0.20. These results indicate the clear contribution of flexural behaviour superimposed on a shear-dominated response that deviates from the ideal shear link.

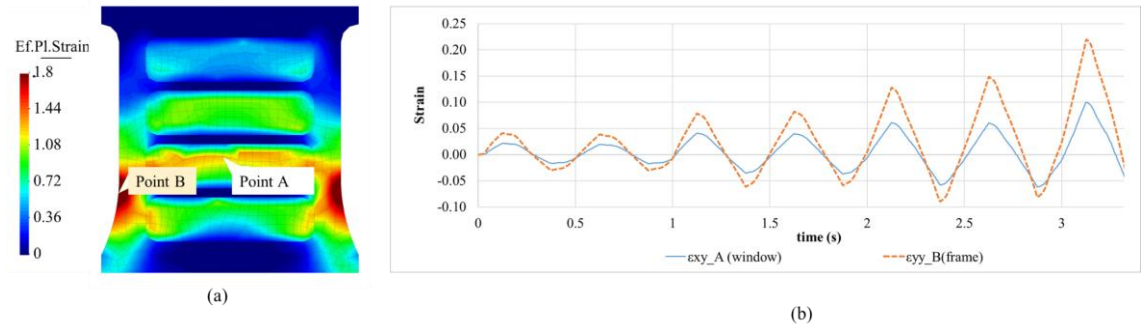

Figure 5 – Local strain response: (a) plastic strain distribution and (b) strain time history

The reference device is initially defined with uniform-thickness windows. However, the final deformation state reveals a non-uniform response among the dissipative windows. Figure 6a shows the distribution of shear strain εxy, where different levels of deformation are observed along the windows. Figure 6b illustrates the relationship between shear strain εxy and shear stress σxy at selected monitoring points. The results indicate that some windows experience higher demand than others, leading to an uneven participation in the dissipation mechanism.

This observation suggests that redistributing the window thickness may improve the structural response. Adjusting the geometry while controlling deformation levels can achieve a more balanced use of the dissipative

capacity. This forms the basis for the optimisation strategy developed in the following sections and highlights opportunities to improve the efficiency of the device.

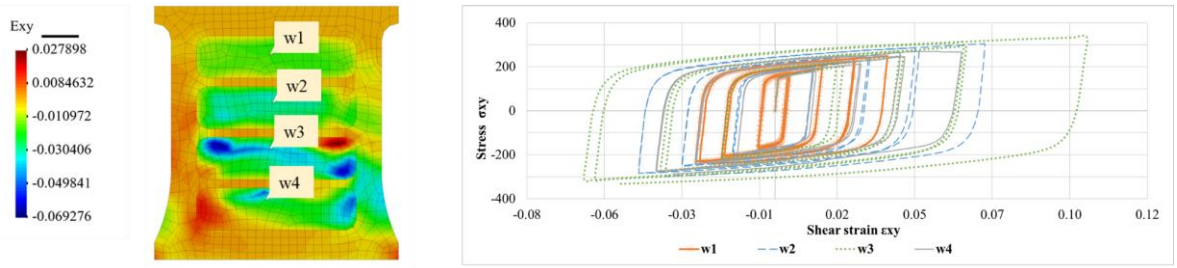

Figure 6 – Shear strain behaviour: (a) εxy field, (b) εxy–σxy curves in windows

4- PARAMETRIC INVESTIGATION OF DAMAGE DISTRIBUTION

The influence of window thickness on the mechanical response and failure-related behaviour of the BDSL system is investigated using a reference configuration denoted as *30_29_3*, which has two windows (see Figure 7a). The parametric variation is defined by modifying the thickness of the dissipative windows between 6 mm and 18 mm. The designation and ordering of the windows follow a top-to-bottom sequence. This range covers practical design limits, from slender configurations with enhanced plastic deformation capacity to thicker windows associated with increased shear stiffness and strength.

All simulations are performed under a displacement-controlled cyclic loading protocol, following ANSI/AISC 341-16 [19] (see Figure 7b), consistent with the previously described experimental methodology.

The loading pattern consists of symmetrical two-cycle sequences with increasing amplitudes, reproducing severe cyclic demand conditions while ensuring consistent comparisons across configurations. All model assumptions, material parameters, and boundary conditions are kept constant, allowing a direct assessment of the influence of window thickness on the global hysteretic response, the distribution of stress triaxiality η expressed through the TFM index, and the concentration of shear and longitudinal plastic strains.

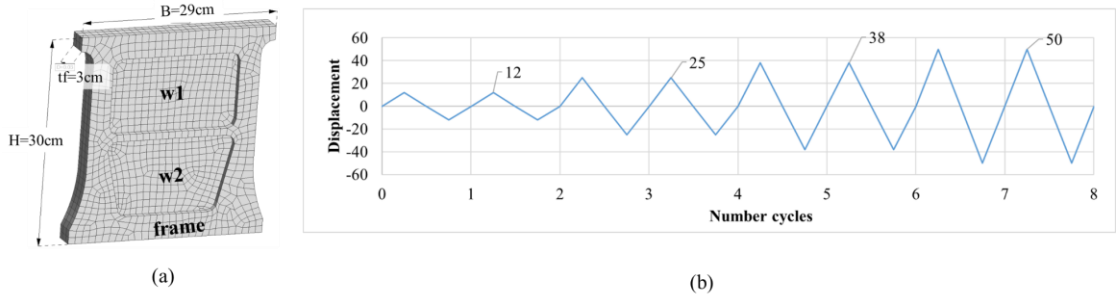

Figure 7 – (a) Geometry and Mesh of BDSL 30_29_3, (b) Displacement-controlled cyclic loading protocol adopted

The window thickness *(tw)* clearly influences both the global hysteretic response and plastic deformation capacity of the system. As *tw* increases, the shear resistance of the windows also increases, resulting in higher force levels and wider hysteretic loops (Figure 8a). Figure 8b shows the corresponding skeleton curves. However, the initial stiffness remains nearly unchanged, since it is primarily governed by the surrounding frame. This behaviour highlights a trade-off between strength and deformation capacity. Thicker windows produce a stronger but less ductile response, as plastic deformation becomes less concentrated in the dissipative regions.

In contrast, thinner windows promote a more pronounced shear-driven plastic response within the windows, enhancing their activation during cyclic loading, although at lower force levels. An excessive reduction in thickness localises deformation, particularly near window corners, resulting in highly concentrated strain fields that compromise structural robustness. Quantitatively, the configuration with *tw = 18 mm* reaches force levels exceeding 600 kN, whereas thinner configurations with *tw = 6 mm* remain around 400 kN under the same loading protocol defined in Figure 7.

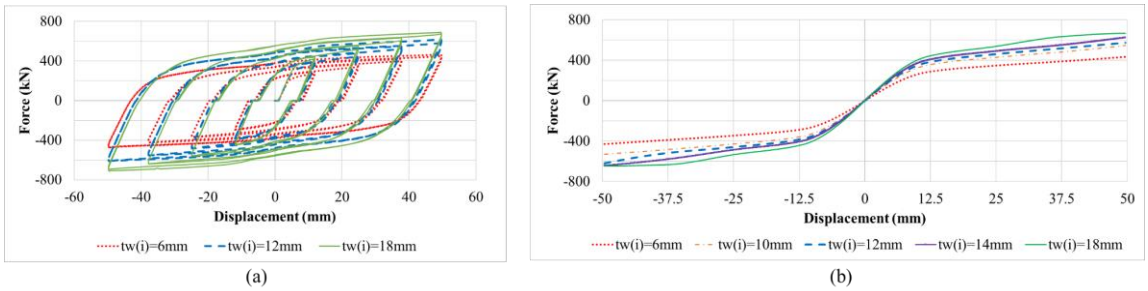

Figure 8 – Influence of window thickness on hysteretic response: (a) hysteretic loops, (b) skeleton curves

Figure 9 presents the distribution of the TFM index, along with the corresponding deformation patterns for different window thicknesses in the analysed geometry. For thicker window configurations, the TFM index remains moderate, with local increases near geometric discontinuities and frame–window transitions, indicating a stress-dominated response. In contrast, thinner windows exhibit higher TFM values, exceeding 100 in critical regions, reflecting a shear-dominated response with greater deformation demand, whereas thicker configurations remain below a reference threshold of 120.

The response is controlled by the interaction between shear mechanisms within the window and normal stress effects in the surrounding frame, leading to non-uniform behaviour. Critical regions consistently appear at the lower corners of the windows, at transition zones, and at the lower part of the frame under large displacement amplitudes. As shown in Figures 9a–c for *tw = 6*, *12*, and *18 mm*, increasing the window thickness reduces the TFM index in the dissipative regions. This behaviour highlights the role of window thickness in controlling the balance between deformation demand and stress status in the dissipative system.

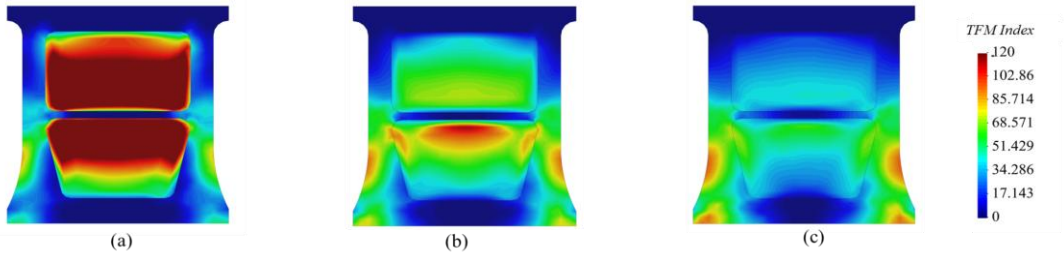

Figure 9 – Effect of window thickness on TFM and Triaxial Failure Response: (a) 6 mm, (b) 12 mm, (c) 18 mm

In addition to the stress state, plastic strain components offer information about the dominant deformation mechanisms. Shear deformation governs the response within the windows, as intended in the design, while longitudinal deformation becomes more relevant as the window thickness increases and the contribution of the frame becomes more significant. In thicker configurations, part of the inelastic demand shifts from the windows to the frame, leading to increased deformation in the lower region and activating areas not intended for energy dissipation.

This work indicates that optimising only the dissipated energy and the TFM index is not sufficient to ensure a controlled distribution of inelastic demand. As shown in Figure 10a, the maximum longitudinal strain in the frame increases progressively, confirming this redistribution, while the TFM index in the frame remains relatively stable within the analysed range.

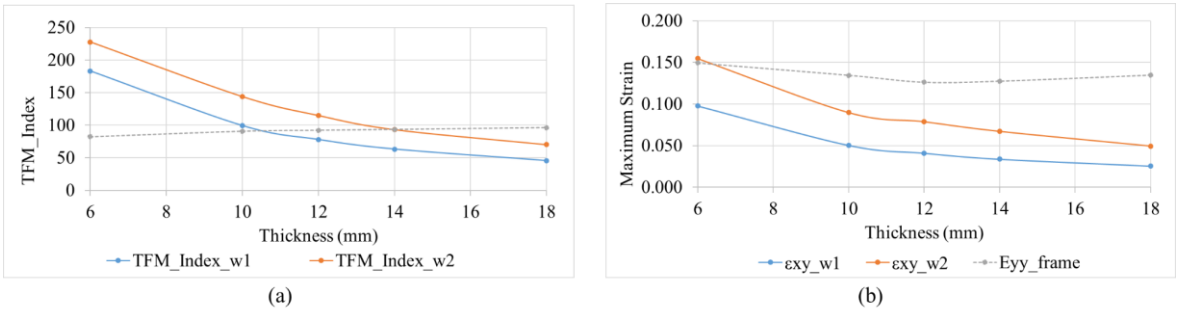

Figure 10 – (a) Evolution of TFM index with thickness (b) variation of Exy and Eyy with thickness

A transition from a window-dominated mechanism to a more distributed response is observed. An intermediate thickness range of approximately 10–14 mm provides a balanced configuration, keeping TFM

within the target range while limiting frame deformation. As shown in Figure 10b, increasing thickness reduces the maximum shear strain in the windows, indicating lower localisation and ductility, while the longitudinal strain in the frame becomes more relevant but remains only weakly sensitive to thickness. Overall, increasing stiffness does not eliminate damage but redistributes the inelastic demand, leading to a less controlled structural response.

5- Optimisation Strategy Based on Energy and Damage Control

The parametric investigation shows that geometric variations strongly influence both global energy dissipation and damage distribution. Therefore, a combined optimisation strategy is proposed, aiming to maximise energy dissipation while ensuring that plastic deformation remains concentrated in the dissipative regions and that damage to the frame is limited.

Two configurations are analysed: *30_34_3* with two windows and *30_29_3* with four windows. The window thickness is selected as the main variable to define the geometric variations, as presented in Section 4, to control stiffness, plastic capacity, and stress-state evolution. Windows are numbered from top to bottom.

The TFM index is evaluated in both the windows and the frame, using the average of the 12 nodes with the highest values. A maximum value of 100 is imposed on the frame to prevent premature damage, while the windows are targeted at 80–90. Some configurations with high energy dissipation show high TFM values in the lower frame, indicating a transfer of inelastic demand and a shift in the deformation mechanism, which reduces structural robustness. In contrast, optimised configurations achieve a balanced response, with the TFM index below the limit in the frame and within the target range in the windows. In these cases, plastic deformation is effectively concentrated in the windows under shear-dominated conditions, while longitudinal deformation in the frame is reduced.

The distribution of the TFM index across different window thicknesses is illustrated in Fig. 11. The TFM in the low-thickness windows *(tw = 6 mm)* exceeds the target range, indicating excessive local demand. Intermediate values *(tw = 12–14 mm)* provide a balanced distribution of inelastic demand, with TFM values within the appropriate range. For higher thickness *(tw = 18 mm)*, the TFM in the windows decreases, while the contribution of the frame increases, indicating a shift in deformation towards the frame. Overall, optimal configurations lead to a more uniform and controlled distribution of inelastic demand. The best balance is obtained at tw = 16 mm for the two-window system *(30_34_3)* and at tw = 14 mm for the four-window configuration *(30_29_3)*, confirming that an intermediate thickness range provides the most efficient response.

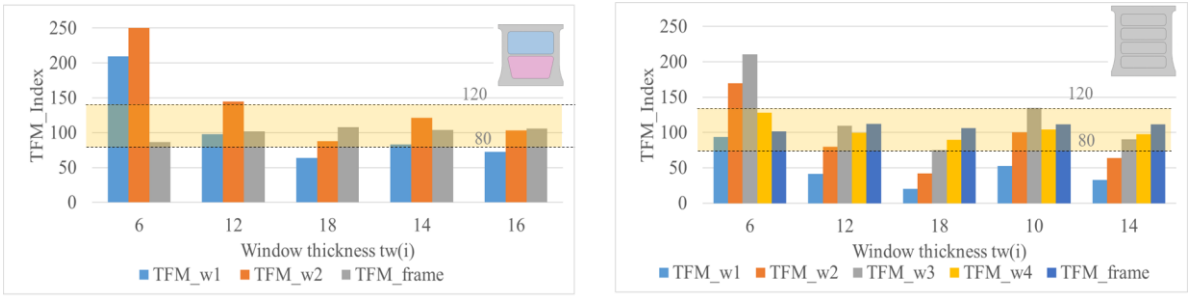

Figure 11 – TFM Index vs. Window Thickness: (a) Two-Window 30_34_3, (b) Four-Window 30_29_3

Stiffness distribution and deformation compatibility explain the improved performance of the optimised configurations, see Fig. 12. Increasing the number of windows leads to a more uniform distribution of shear deformation along the height of the device, reducing strain concentration at geometric discontinuities. At the same time, the appropriate window thickness prevents excessive softening and limits localisation effects. In the two-window configuration, the wider window increases shear demand within each dissipative region, potentially increasing the equivalent plastic strain and promoting the transfer of stress concentrations towards the frame. Conversely, the four-window arrangement distributes inelastic demand more evenly, maintaining stress triaxiality within acceptable levels while preserving energy-dissipation capacity.

Likewise, the influence of thickness distribution on the TFM index in the dissipative regions and the surrounding frame is illustrated in Fig. 13. Figures 13a and 13b present the distribution of the TFM index in the windows for the two- and four-window configurations (*2W*, *4W*), respectively. In uniform-thickness cases, the TFM index is unevenly distributed, with certain windows reaching higher values, indicating inefficient activation of the dissipative system.

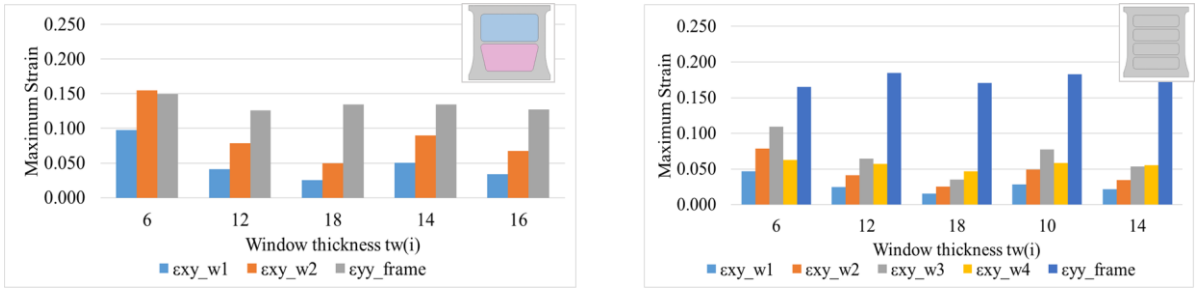

Figure 12 – Maximum Strain (a) Two-Window 30_34_3, (b) Four-Window 30_29_3

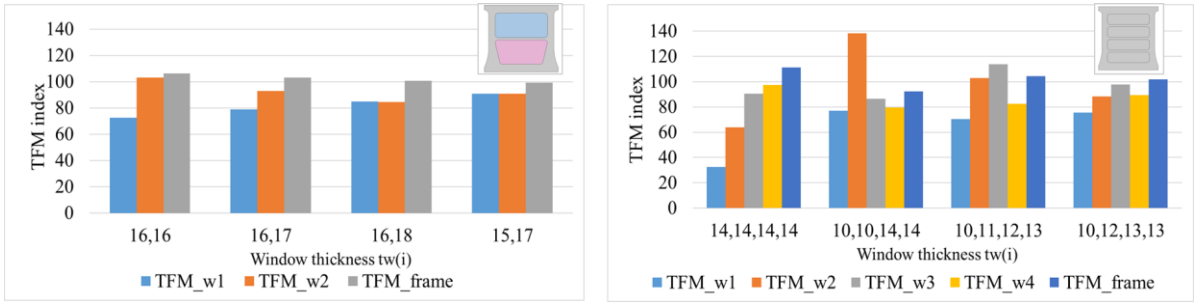

Figure 13 – Effect of Window Thickness Variation on TFM: (a) 2W 30_34_3, (b) 4W 30_29_3

In contrast, after tuning the window thickness based on the TFM optimisation criteria, the shear strain becomes more evenly distributed across all windows, reducing differences in deformation levels and enhancing the involvement of each dissipative region in multi-window configurations. At the same time, the longitudinal strain in the frame (εyy) remains relatively stable, indicating that the redistribution occurs primarily within the window system; see Figure 14.

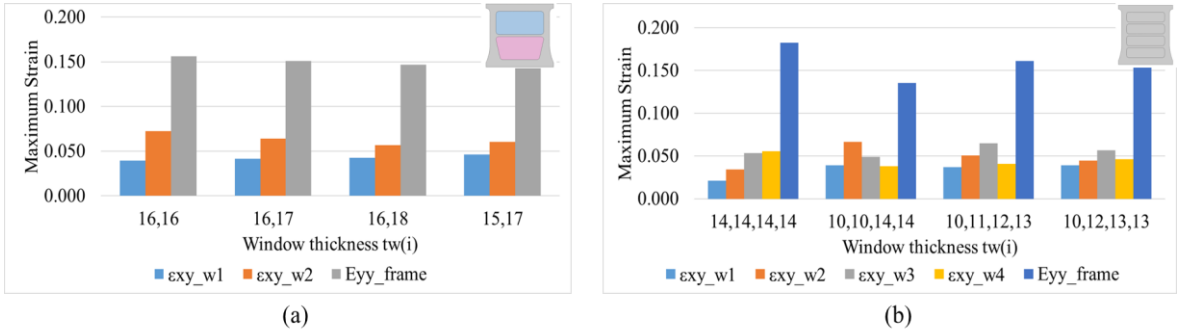

Figure 14 – Shear and longitudinal strain distribution for variable window thickness configurations

This behaviour shows that a geometric refinement of the window thickness leads to a more uniform distribution of inelastic demand and a more efficient activation of the intended plastic mechanisms. In contrast, uniform configurations exhibit non-uniform behaviour, characterised by localised deformation and inefficient use of the available dissipative capacity, whereas the TFM index enables the identification of critical regions and supports the optimisation process.

The optimal BDSL configurations and their corresponding TFM distributions are illustrated in Fig. 15. Compared to the uniform designs, the optimised cases exhibit a more uniform distribution of the TFM index, reduced peak values, and a more balanced activation of the dissipative windows. The geometric redistribution mitigates critical regions and enhances deformation uniformity, confirming the effectiveness of variable window thickness in controlling local damage and improving performance.

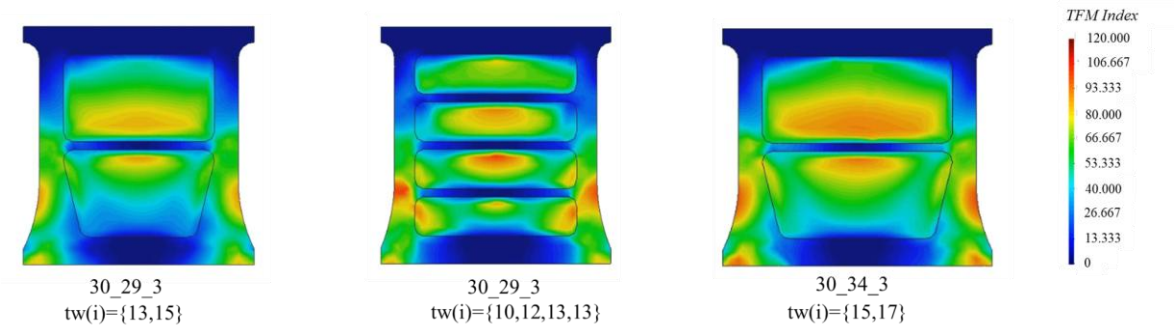

Figure 15 – TFM distribution in optimised BDSL configurations with variable window thickness

Overall, varying window thickness enhances the structural response by promoting a more uniform distribution of deformation, reducing local damage, and limiting the contribution of the frame. The optimal configurations effectively concentrate inelastic demand in the dissipative regions, achieving a balanced behaviour. The combined use of energy-based and TFM-based criteria provides a consistent framework for achieving more robust and controlled designs.

6- CONCLUSIONS

This study proposes a methodology that integrates energy dissipation and damage control for Buckling-Delayed Shear Link systems subjected to cyclic loading. The results show that both window thickness and the number of windows strongly influence cumulative energy dissipation and the spatial distribution of inelastic demand. High energy dissipation alone does not guarantee controlled behaviour; certain configurations lead to increased TFM index values in the frame, indicating an undesirable demand transfer. The Triaxial Failure Map provides a consistent basis to distinguish between beneficial deformation concentrated in the windows and critical conditions affecting the surrounding frame. An optimal response is achieved when the frame remains below the defined TFM threshold and the windows operate within a controlled utilisation range. Overall, the proposed optimisation approach enhances structural robustness by balancing global hysteretic performance with local damage control.

The conclusions of this study are restricted to the calibrated ASTM A36 material model, the analysed geometric families, and the imposed cyclic loading protocol. Since the TFM is used here as a post-processing indicator rather than as a constitutive fracture model, experimental validation of the optimised configurations remains necessary before broader design recommendations can be established.

7- ACKNOWLEDGMENT

The authors acknowledge the financial support of the Project ACE100/23/000022 – Edificacions resilients equipades amb dissipadores Shear Link, funded by the Government of Catalonia through ACCIÓ and with the support of the Catalan Office for Climate Change, with the participation of Luis Bozzo Estructuras y Proyectos S.L. and the Centre Internacional en Mètodes Numèrics a l'Enginyeria (CIMNE).

8- REFERENCES

[1] Malley, J. O., Popov, E. P.: Shear links in eccentrically braced frames, in: *Journal of Structural Engineering*, ASCE Volume 110, no. 9, 1984, pp. 2275–2295. https://doi.org/10.1061/(ASCE)0733-9445(1984)110:9(2275)

[2] Okazaki, T., Engelhardt, M. D.: Cyclic loading behavior of EBF links constructed of ASTM A992 steel, in: *Journal of Constructional Steel Research* Volume 63, no. 6, 2007, pp. 751–765. https://doi.org/10.1016/j.jcsr.2006.08.004

[3] Kanvinde, A. M., Deierlein, G. G.: Cyclic void growth model to assess ductile fracture initiation in structural steels due to ultra low cycle fatigue, in: *Journal of Engineering Mechanics*, ASCE Volume 133, no. 6, 2007, pp. 701–712. https://doi.org/10.1061/(ASCE)0733-9399(2007)133:6(701)

[4] Rice, J. R., Tracey, D. M.: On the ductile enlargement of voids in triaxial stress fields, in: *Journal of the Mechanics and Physics of Solids* Volume 17, no. 3, 1969, pp. 201–217. https://doi.org/10.1016/0022-5096(69)90033-7

[5] Bao, Y., Wierzbicki, T.: On fracture locus in the equivalent strain and stress triaxiality space, in: *International Journal of Mechanical Sciences* Volume 46, no. 1, 2004, pp. 81–98. https://doi.org/10.1016/j.ijmecsci.2004.02.006
[6] Wierzbicki, T., Bao, Y., Lee, Y.-W., Bai, Y.: Calibration and evaluation of seven fracture models, in: *International Journal of Mechanical Sciences* Volume 47, no. 4–5, 2005, pp. 719–743. https://doi.org/10.1016/j.ijmecsci.2005.03.003
[7] Bai, Y., Wierzbicki, T.: A new model of metal plasticity and fracture with pressure and Lode dependence, in: *International Journal of Plasticity* Volume 24, no. 6, 2008, pp. 1071–1096. https://doi.org/10.1016/j.ijplas.2007.09.004
[8] Ramírez M., J., Bozzo, G., Gonzalez, J. M., Rastellini, F. G., Irazábal, J., Bozzo, L.: Advanced modeling of buckling delayed shear links under strong cyclic loads, in: *COMPDYN 2025: 10th International Conference on Computational Methods in Structural Dynamics and Earthquake Engineering*, Rhodes Island, Greece, 2025.
[9] Ramírez M., J., Bozzo, G., Rastellini, F. G., Gonzalez, J. M., La Torre, D., Almeida, A., Valcárcel, E.: Advances in the design of energy dissipating devices: experimental and numerical characterization, in: *18th World Conference on Earthquake Engineering (WCEE 2024)*, Milan, Italy, 2024. No DOI located.
[10] Rastellini, F., Socorro, G., Forgas, A., Oñate, E.: A triaxial failure diagram to predict the forming limit of 3D sheet metal parts subjected to multiaxial stresses, in: *Journal of Physics: Conference Series* Volume 734, no. 3, 2016, Article 032020. https://doi.org/10.1088/1742-6596/734/3/032020
[11] Bozzo Rotondo, L. M., Bozzo Fernández, G.: *Buckling delayed shear link*, U.S. Patent 12,180,741 B2, filed as U.S. Patent Application No. 17/967,199; prior publication US 2024/0125137 A1, 2024.
[12] Bozzo, G., Perez, L., Miranda, E., Báiran, J., Bozzo, L.: Optimal set-up configuration for testing stiff energy-dissipating devices under large displacements, in: *18th World Conference on Earthquake Engineering (WCEE 2024)*, Milan, Italy, 2024.
[13] Rastellini, F., Oller, S., Salomón, O., Oñate, E.: Composite materials non-linear modelling for long fibre-reinforced laminates: continuum basis, computational aspects and validations, in: *Computers & Structures* Volume 86, no. 9, 2008, pp. 879–896. https://doi.org/10.1016/j.compstruc.2007.04.009
[14] Flores, F. G.: A simple reduced integration hexahedral solid-shell element for large strains, in: *Computer Methods in Applied Mechanics and Engineering* Volume 303, 2016, pp. 260–287. https://doi.org/10.1016/j.cma.2016.01.013
[15] Yoshida, F., Uemori, T., Fujiwara, K.: Elastic–plastic behavior of steel sheets under in-plane cyclic tension–compression at large strain, in: *International Journal of Plasticity* Volume 18, no. 5–6, 2002, pp. 633–659. https://doi.org/10.1016/S0749-6419(01)00049-3
[16] Jia, L. J., Kuwamura, H.: Prediction of cyclic behaviors of mild steel at large plastic strain using coupon test results, in: *Journal of Structural Engineering*, ASCE Volume 140, no. 2, 2014, Article 04013056. https://doi.org/10.1061/(ASCE)ST.1943-541X.0000848
[17] Zhong, Z.-H.: *Finite Element Procedures for Contact-Impact Problems*, Oxford University Press, Oxford, 1993. https://doi.org/10.1093/oso/9780198563839.001.0001
[18] Zhuang, C., Mu, L., Zhang, J., Jiang, R., Jia, Z.: Ductile fracture characterization of A36 steel and comparative study of phenomenological models, in: *Journal of Materials in Civil Engineering*, ASCE Volume 33, no. 1, 2021, Article 04020421. https://doi.org/10.1061/(ASCE)MT.1943-5533.0003543
[19] American Institute of Steel Construction: *Seismic Provisions for Structural Steel Buildings*, ANSI/AISC 341-16, Chicago, IL, July 12, 2016.